Letter

Ultrafast magnetization dynamics in the half-metallic Heusler alloy Co_2FeAl

R. S. Malik,[1] E. K. Delczeg-Czirjak,[1] R. Knut,[1] D. Thonig,[3] I. Vaskivskyi,[1] D. Phuyal,[1,2] R. Gupta,[4] S. Jana,[1] R. Stefanuik,[1] Y. O. Kvashnin,[1] S. Husain,[4] A. Kumar,[4] P. Svedlindh,[4] J. Söderström,[1] O. Eriksson,[1,3] and O. Karis[1]

[1]*Department of Physics and Astronomy, Uppsala University, Box 516, SE-75120 Uppsala, Sweden*

[2]*Department of Applied Physics, KTH Royal Institute of Technology, SE-106 91 Stockholm, Sweden*

[3]*School of Science and Technology, Örebro University, SE-70182 Örebro, Sweden*

[4]*Department of Materials Science and Engineering, Uppsala University, Box 534, SE-75121 Uppsala, Sweden*

(Received 1 March 2020; revised 24 August 2021; accepted 24 August 2021; published 14 September 2021; corrected 23 March 2022)

We report on optically induced, ultrafast magnetization dynamics in the Heusler alloy Co_2FeAl, probed by time-resolved magneto-optical Kerr effect. Experimental results are compared to results from electronic structure theory and atomistic spin-dynamics simulations. Experimentally, we find that the demagnetization time (τ_M) in films of Co_2FeAl is almost independent of varying structural order, and that it is similar to that in elemental 3*d* ferromagnets. In contrast, the slower process of magnetization recovery, specified by τ_R, is found to occur on picosecond time scales, and is demonstrated to correlate strongly with the Gilbert damping parameter (α). Based on these results we argue that for Co_2FeAl the remagnetization process is dominated by magnon dynamics, something which might have general applicability.

DOI: 10.1103/PhysRevB.104.L100408

Studies of ultrafast demagnetization was pioneered by Beaurepaire *et al.* [1], who demonstrated that the optical excitation of a ferromagnetic material, using a short pulsed laser, could quench the magnetic moment on subpicosecond time scales. The exact underlying microscopic mechanisms responsible for the transfer of angular momentum have been strongly debated for more than 20 years [2–4]. Ultrafast laser-induced demagnetization has now become an intense field of research not only from fundamental point of view but also from a technological aspect, due to an appealing possibility to further push the limits of operation of information storage and data processing devices [5]. Both experiment [4–15] and theory [16–23] report that all of the 3*d* ferromagnets (Fe, Ni, and Co) and their alloys, show characteristic demagnetization times in the subpicosecond range, while 4*f* metals exhibit a complicated two-step demagnetization up to several picoseconds after the excitation pulse [4,24].

In this paper, we have made element specific investigations of the ultrafast magnetization dynamics of a half-metallic Heusler alloy. The half-metallic Heusler alloys have a unique electronic structure, where the majority spin-channel has a metallic character while the minority spin-channel has a band gap and ideally exhibit 100% spin-polarization at the Fermi level.

Heusler alloys are also appealing for spintronic applications due to the low Gilbert damping, which is related with the half-metallicity [25,26]. The origin of the band gap and the mechanism of half-metallicity in these materials have been studied by using first-principle electronic structure calculations [27–30].

The half-metallic property is furthermore known to be very sensitive to structural disorder [28–32]. From a fundamental point of view, it is intriguing to ask, how the band gap in the minority spin channel effects the ultrafast magnetization dynamics of Heusler alloys [33,34]. It has already been reported that some of the half-metals like CrO_2 and Fe_3O_4 exhibit very slow dynamics, involving time scales of hundreds of picoseconds [33,34], while several Co-based Heusler alloys show a much faster demagnetization, similar to the time scales of the elemental 3*d* ferromagnets [35–37]. The faster dynamics of these Heuslers has been discussed in Ref. [33] to be due to the fact that the band gap in the minority spin channel is typically around $0.3 - 0.5$ eV, which is smaller than the photon energy (1.5 eV) of the exciting laser. It is also smaller than the band gap of CrO_2 and Fe_3O_4. Importantly, the Heusler alloys offer the possibility to study magnetization dynamics, as a function of structural order, since they normally can be prepared to have a fully ordered $L2_1$ phase, a partially ordered $B2$ phase, and a completely disordered $A2$ phase. The structural relationships of these phases are described within the Supplemental Material (SM) [38].

We have here studied the optically induced, ultrafast magnetization dynamics of Co_2FeAl (CFA) films, using time-resolved magneto-optical Kerr effect (TR-MOKE) as described in Ref. [39,68,69]. By control of the growth temperature, CFA alloy forms with varying degree of structural order, in a continuous way between the $A2$ and $B2$ phases, as well as between the $B2$ and $L2_1$ phases [40,41]. We present data from four CFA samples, grown at 300K, 573K, 673K, and 773 K, respectively. We henceforth denote each sample by its growth temperature as a subscript, e.g., CFA_{300K}. As evidenced by x-ray diffraction, the sample grown at 300 K is found to exhibit

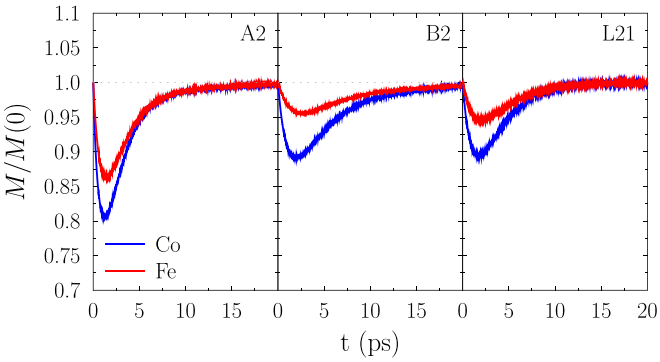

FIG. 1. Simulations of ultrafast dynamics of Co_2FeAl in the different structural phases $A2$ (left panel), $B2$ (central panel), and $L2_1$ (right panel). The demagnetization is shown element resolved (blue line, Co; red line, Fe). The peak temperature in the 2TM model is 1200 K. The dotted line indicates the equilibrium magnetization at $T = 300$ K.

the A2 phase, while the samples grown at 573 K, 673 K, and 773 K predominantly exhibit the B2 phase [41]. The value of the Gilbert damping α is found to monotonously decrease with annealing temperature and is thus lowest for the sample grown at 773 K [42].

Calculations based on density functional theory (DFT) of the magnetic moment, Heisenberg exchange interaction, and the Gilbert damping parameter are described in detail in Sec. S1 of Supplemental Material (SM) [38], which includes Refs. [43–57]. These parameters were used in a multiscale approach to perform atomistic magnetization dynamics simulations, described in Sec. S2 of SM [38], which includes Ref. [58]. Here we employed a slight modification of the three temperature model (3TM), as was proposed in Ref. [1], in fact as a generalization of a pioneering study of an electron-lattice model, published in Ref. [59]. As outlined in Sec. S2 of SM [38], this allows for an estimate of the temperature profile of the spin-system, of all alloys investigated here. In the 2TM, the spin temperature increases due to the coupling to the hot-electron bath, that is excited by the external laser pulse. In the simulations we used a peak temperature in the 2TM of 1200 K. A full description of the 2TM and the details of all spin-dynamics simulations are described in Sec. S2 of SM [38].

The results of the simulations are shown in Fig. 1, for the $A2$, $B2$, and $L2_1$ phases. It can be seen that the different phases react differently to the external stimulus. In general, this model provides a dynamics that is controlled by (i) the temperature of the spin subsystem, (ii) the strength of the magnetic exchange interaction, and (iii) the dissipation of angular momentum and energy during the relaxation of the atomic magnetic moments (Gilbert damping) [60]. Before continuing the discussion, we note that the average magnetization M of element X is calculated as $M^X = \sum_i c_i^X M_i^X / 4 \sum_i c_i^X$, where c_i^X is the concentration of the particular element X in the particular phase and i runs over the four nonequivalent sites of the unit cell. After the material demagnetizes, the spin temperature eventually drops and the average magnetization returns to its initial value after $10 - 20$ ps (cf. Fig. 1).

To estimate the time constants of the demagnetization (τ_M) and remagnetization (τ_R) processes, in an element-specific

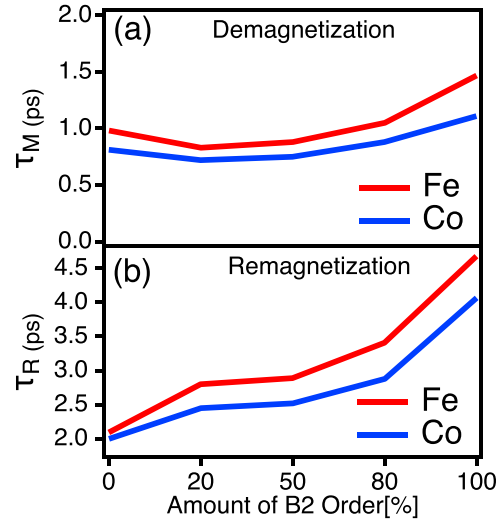

FIG. 2. Element resolved relaxation times of Co_2FeAl, from simulations of alloys with varying amounts of $A2 \rightarrow B2$ phase. 0 corresponds to pure $A2$ phase while 100 corresponds to pure $B2$ phase. Panel (a) shows the demagnetization time and panel (b) shows the remagnetization time. Both time constants are obtained from fitting the time trajectory of $M^X(t)$ by a double-exponential function (see text).

way, we fit both the theoretical and experimental transient magnetizations by a double exponential function [61]. We show results of τ_M and τ_R in Fig. 2 for the $A2$ and $B2$ phase, as well as for alloys with intermediate degree of disorder (described in Sec. S2 of SM [38]).

The theoretical demagnetization time is seen from Fig. 2 to typically be around 1 ps, whereas the remagnetization time is $2 - 5$ ps. In the theoretical data of Fig. 2, it can be seen that as the $B2$ ordering increases (moving to the right along the x axis), both the demagnetization and remagnetization times increases. However, the simulations show a stronger increase of the remagnetization time as function of $B2$ ordering. We also note that the relevant time scale is somewhat larger for Fe than for Co, and the ratio between them τ_{Fe}/τ_{Co} grows when going from $A2$ to $B2$ phase.

Figures 3(a)–3(d) shows the element specific magnetization dynamics of CFA films that have different structure ordering, depending on their growth temperatures. All of the measurements are conducted in a time-resolved transverse magneto-optical Kerr effect (TR-MOKE) spectrometer. (For details, see SM [38], Sec. S3 for thin films synthesis, which includes Refs. [62,63], and Sec. S4 for the experimental setup and measurements, which includes Refs. [64–69]). The inset of Fig. 3 shows the observed magnetization dynamics up to ~1 ps. All of the films are demagnetized (~25%) with a similar pump fluence. For all samples, the data for Fe (red) and Co (blue) show similar demagnetization dynamics in the first few hundred femtoseconds, whereupon differences in the remagnetization dynamics become visible, especially on the picosecond time scale. A significant change in the remagnetization dynamics is more obvious for the film with $A2$ phase in Fig. 3(a) and film with 83% $B2$ phase in Fig. 3(d). Figure 4(a)–4(b) shows the measured values of the demagnetization and remagnetization time constants, for the four

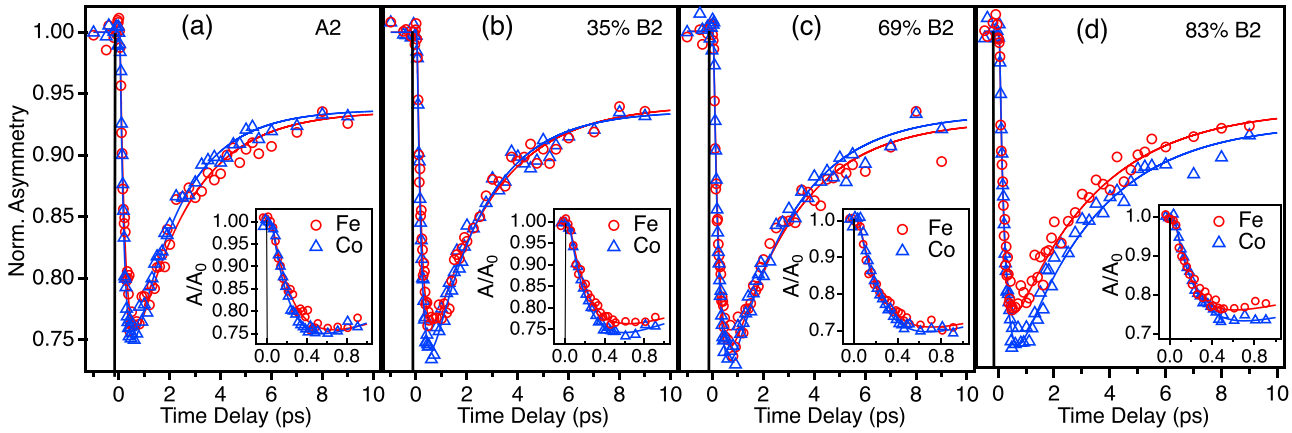

FIG. 3. Measured element-specific Fe (red) and Co (blue) magnetization dynamics of Co_2FeAl. Samples are denoted by the growth temperature in each case. The red and blue lines correspond to fitted data (see text). (a) 300 K ($A2$ phase), (b) 573 K (35% $B2$ phase), (c) 673 K (69% $B2$ phase), and (d) 773 K (83% $B2$ phase). The insets show the demagnetization dynamics up to ∼1ps. All of the measurements were performed with similar pump fluence (for details, see Sec. S4 of SM).

different growth temperatures, representing different degree of order in Co_2FeAl, along the path $A2 \rightarrow B2$. It may be seen that the τ_M for Fe and Co is the same within the error bars for all four samples, regardless of the degree of structural ordering [Fig. 4(a)]. It may also be noted that the measured τ_M for CFA is similar to that of 3d transition metals [35,36] and very much shorter than that of CrO_2 or Fe_3O_4.

Demagnetization times that are independent on degree of structural ordering is interesting, since it can be expected that the presence of structural disorder in Heusler alloys ought to result in a lower degree of spin polarization of the electronic states (i.e., an increased density of states (DOS) at the Fermi level in the minority band). This is expected to enhance spin-flip scattering, with an accompanying speed-up of the demagnetization dynamics [33,34]. The electronic structure calculation of CFA also shows that the DOS at the Fermi level varies with different structural phases (analyzed in Sec. S1 of SM [38]). The $A2$ phase has a large number of states at the Fermi level, while the $L2_1$ phase, and to some extent the $B2$ phase, has a low amount [41]. Despite these differences in the electronic structure, the measured demagnetization dynamics shown in Fig. 4(a) is essentially independent on degree of structural ordering.

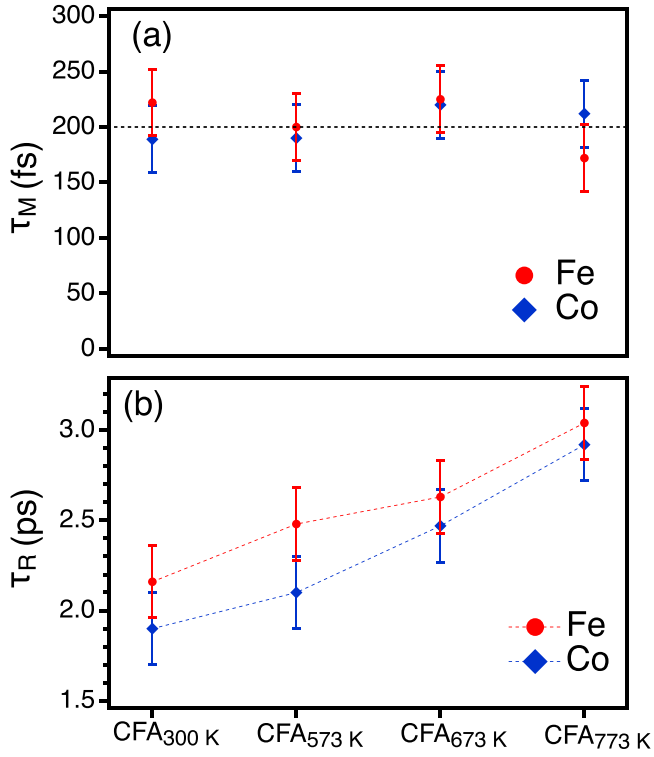

FIG. 4. Measured magnetization times for the investigated Co_2FeAl alloys. In (a) the demagnetization time τ_M is shown and in (b) the remagnetization time τ_R is plotted.

On longer time scales, there is a significant effect of structural ordering on the observed magnetization dynamics, which becomes particularly relevant for the remagnetization process. As seen in Fig. 4(b), there is a monotonous increase of remagnetization time τ_R with increasing growth temperature and hence the degree of ordering along the $A2 \rightarrow B2$ path. The sample grown at 300 K with $A2$ phase, exhibits the fastest remagnetization dynamics (τ_R). With increasing growth temperature and corresponding increase in the structural ordering along the $A2 \rightarrow B2$ path, a distinct trend of increasingly slower remagnetization dynamics is observed. We expect the thermal conductivity to increase with increasing B2 ordering. This would result in a faster recovery of the electronic temperature and hence a faster remagnetization time with increasing B2 order. To verify this, we calculated the Debye temperature for different B2 ordering and found it to change negligibly (∼4%), indicating that the phonon mediated thermal conductivity is almost sample independent [70]. The electron-mediated thermal conductivity is given by Wiedeman-Franz law, which describes a proportional relationship between the electrical conductivity and the electronic heat conductivity. The electrical conductivity decreases significantly (∼30%) with increasing disorder in this alloy [71]. Since a decreased heat conductivity should result in a slower remagnetization, changes in the heat diffusion cannot explain the observed trend where the remagnetization becomes faster with increasing disorder and decreasing conductivity. The most conspicuous behavior of

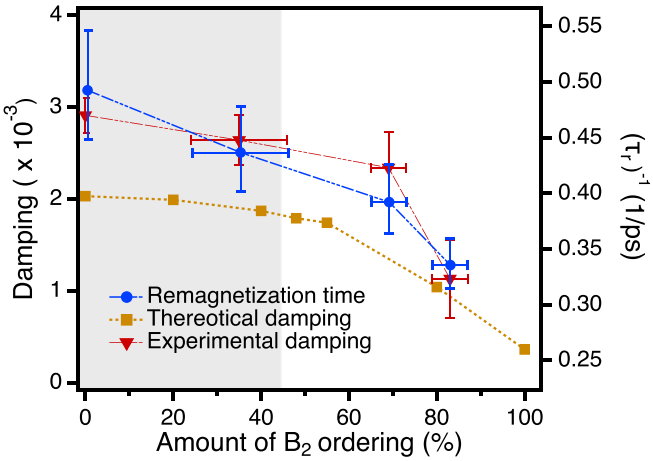

FIG. 5. The relationship of inverse of the measured remagnetization time (right y axis) and theoretically calculated and experimentally measured Gilbert damping (left y axis) in Co_2FeAl for varying amount of B2 order along the $A2 \rightarrow B2$ path, i.e., 0 corresponds to pure A2 phase while 100 corresponds to pure B2 phase. The CFA_{300K} sample shows no visible ordering peak in XRD and can only be determined to be within the shaded region (cf. Sec. S3 of SM [38]).

the measured magnetization dynamics, and its dependence on the degree of ordering, concerns the remagnetization time [Fig. 4(b)].

The time scale of the remagnetization process is sufficiently long to allow for an interpretation based on atomistic spin dynamics. Two materials specific parameters should be the most relevant to control this dynamics; the exchange interaction, as revealed by the local Weiss field, and the damping parameter. In Sec. S2 of SM [38], we report on the calculated Weiss fields and damping parameters. It is clear from these results that the trend in the experimental data shown in Fig. 4(b), can not be understood from the Weiss field alone, whereas an explanation based on the damping is more likely. In order to illustrate this, we show in Fig. 5 the inverse of the measured remagnetization time compared to the theoretically calculated damping and experimentally measured damping (intrinsic) through ferromagnetic resonance (FMR) (described in Sec. S6 of SM [38], which includes Ref. [72]). The figure shows that the damping is large in the completely disordered *A*2 phase and for a large range of structural orderings, which comes out from both theory and experiment. The figure also demonstrates that the inverse of the measured remagnetization time scales very well with both the calculated damping and experimentally measured damping. According to the figure, a large damping parameter corresponds to faster remagnetization dynamics in the measurements.

Co_2FeAl is, to the best of our knowledge, the first system where experimental observations and theory point to the importance of damping in the process of ultrafast magnetization dynamics. We note that this primarily is relevant for the remagnetization process; the initial part of the magnetization dynamics (first few hundred fs) is distinctly different. In the element resolved demagnetization, we observe a similar behavior for Fe and Co in all samples, and an insensitivity of the demagnetization times in relation to structural ordering. This does not agree with atomistic spin-dynamics simulations, that show distinctly different behavior between the elements and a sensitivity to structural ordering. Also, since the demagnetization times are significantly different between the experiment and simulations, other mechanisms, of electronic origin, most likely play role in this temporal regime.

The remagnetization process of Co_2FeAl alloy with varying degree of structural order, highlights clearly the importance of the Gilbert damping and that magnon dynamics dominates the magnetization at ps time scales. The relevance of the Gilbert damping parameter for ps dynamics is natural, since this controls angular momentum (and energy) transfer to the surrounding. What is surprising with Co_2FeAl is the fact that other interactions (e.g., the Weiss field) show such a weak dependence on the amount of structural disorder. This is fortuitous, since it allows to identify the importance of the Gilbert damping. A picture emerges from the results presented here, that the magnetization dynamics in general have two regimes; one which is primarily governed by electronic processes, and is mainly active in the first few hundred fs (τ_M), and a second regime where it is primarily magnons that govern the remagnetiztion dynamics (τ_R).

We acknowledge support from the Swedish Research Council (VR, Contract No. 2020-00681, No. 2019-03666,2017-03799, No. 2016-04524, and No. 2013-08316), the Swedish Foundation for Strategic Research, project SSF Magnetic materials for green energy technology under Grant No. EM16-0039, the Knut and Alice Wallenberg foundation, STandUP and eSSENCE, for financial support. The Swedish National Infrastructure for Computing (SNIC) is acknowledged for computational resources.

[1] E. Beaurepaire, J.-C. Merle, A. Daunois, and J.-Y. Bigot, Phys. Rev. Lett. **76**, 4250 (1996).

[2] A. Scholl, L. Baumgarten, R. Jacquemin, and W. Eberhardt, Phys. Rev. Lett. **79**, 5146 (1997).

[3] B. Koopmans, J. J. M. Ruigrok, F. D. DallaLonga, and W. J. M. de Jonge, Phys. Rev. Lett. **95**, 267207 (2005).

[4] B. Koopmans, G. Malinowski, F. Dalla Longa, D. Steiauf, M. Fähnle, T. Roth, M. Cinchetti, and M. Aeschlimann, Nat. Mater. **9**, 259 (2010).

[5] A. Kirilyuk, A. V. Kimel, and T. Rasing, Rev. Mod. Phys. **82**, 2731 (2010).

[6] M. Cinchetti, M. Sánchez Albaneda, D. Hoffmann, T. Roth, J.-P. Wüstenberg, M. Krauß, O. Andreyev, H. C. Schneider, M. Bauer, and M. Aeschlimann, Phys. Rev. Lett. **97**, 177201 (2006).

[7] C. Stamm, T. Kachel, N. Pontius, R. Mitzner, T. Quast, K. Holldack, S. Khan, C. Lupulescu, E. Aziz, M. Wietstruk *et al.*, Nat. Mater. **6**, 740 (2007).

[8] F. Dalla Longa, J. T. Kohlhepp, W. J. M. de Jonge, and B. Koopmans, Phys. Rev. B **75**, 224431 (2007).

[9] J. Walowski, G. Müller, M. Djordjevic, M. Münzenberg, M. Kläui, C. A. F. Vaz, and J. A. C. Bland, Phys. Rev. Lett. **101**, 237401 (2008).

[10] E. Carpene, E. Mancini, C. Dallera, M. Brenna, E. Puppin, and S. De Silvestri, Phys. Rev. B **78**, 174422 (2008).

[11] T. Roth, A. J. Schellekens, S. Alebrand, O. Schmitt, D. Steil, B. Koopmans, M. Cinchetti, and M. Aeschlimann, Phys. Rev. X **2**, 021006 (2012).

[12] S. Mathias, C. La-O-Vorakiat, P. Grychtol, P. Granitzka, E. Turgut, J. M. Shaw, R. Adam, H. T. Nembach, M. E. Siemens, S. Eich *et al.*, Proc. Natl. Acad. Sci. USA **109**, 4792 (2012).

[13] D. Rudolf, C. La-O-Vorakiat, M. Battiato, R. Adam, J. M. Shaw, E. Turgut, P. Maldonado, S. Mathias, P. Grychtol, H. T. Nembach *et al.*, Nat. Commun. **3**, 1037 (2012).

[14] A. Eschenlohr, M. Battiato, P. Maldonado, N. Pontius, T. Kachel, K. Holldack, R. Mitzner, A. Föhlisch, P. M. Oppeneer, and C. Stamm, Nat. Mater. **12**, 332 (2013).

[15] E. Turgut, C. La-o vorakiat, J. M. Shaw, P. Grychtol, H. T. Nembach, D. Rudolf, R. Adam, M. Aeschlimann, C. M. Schneider, T. J. Silva, M. M. Murnane, H. C. Kapteyn, and S. Mathias, Phys. Rev. Lett. **110**, 197201 (2013).

[16] G. P. Zhang and W. Hübner, Phys. Rev. Lett. **85**, 3025 (2000).

[17] B. Koopmans, H. Kicken, M. Van Kampen, and W. De Jonge, J. Magn. Magn. Mater. **286**, 271 (2005).

[18] M. Krauß, T. Roth, S. Alebrand, D. Steil, M. Cinchetti, M. Aeschlimann, and H. C. Schneider, Phys. Rev. B **80**, 180407(R) (2009).

[19] D. Steiauf and M. Fähnle, Phys. Rev. B **79**, 140401(R) (2009).

[20] J.-Y. Bigot, M. Vomir, and E. Beaurepaire, Nat. Phys. **5**, 515 (2009).

[21] M. Battiato, K. Carva, and P. M. Oppeneer, Phys. Rev. Lett. **105**, 027203 (2010).

[22] S. Essert and H. C. Schneider, Phys. Rev. B **84**, 224405 (2011).

[23] U. Atxitia and O. Chubykalo-Fesenko, Phys. Rev. B **84**, 144414 (2011).

[24] I. Radu, C. Stamm, A. Eschenlohr, F. Radu, R. Abrudan, K. Vahaplar, T. Kachel, N. Pontius, R. Mitzner, K. Holldack *et al.*, SPIN **05**, 1550004 (2015).

[25] J. M. Shaw, E. K. Delczeg-Czirjak, E. R. J. Edwards, Y. Kvashnin, D. Thonig, M. A. W. Schoen, M. Pufall, M. L. Schneider, T. J. Silva, O. Karis, K. P. Rice, O. Eriksson, and H. T. Nembach, Phys. Rev. B **97**, 094420 (2018).

[26] C. Liu, C. K. Mewes, M. Chshiev, T. Mewes, and W. H. Butler, Appl. Phys. Lett. **95**, 022509 (2009).

[27] I. Galanakis, P. H. Dederichs, and N. Papanikolaou, Phys. Rev. B **66**, 174429 (2002).

[28] I. Galanakis and P. Mavropoulos, J. Phys: Cond. Matter. **19**, 315213 (2007).

[29] M. I. Katsnelson, V. Y. Irkhin, L. Chioncel, A. I. Lichtenstein, and R. A. de Groot, Rev. Mod. Phys. **80**, 315 (2008).

[30] H. C. Kandpal, G. H. Fecher, and C. Felser, J. Phys. D **40**, 1507 (2007).

[31] B. Balke, S. Wurmehl, G. H. Fecher, C. Felser, and J. Kübler, Sci. Tech. Adv. Mater. **9**, 014102 (2008).

[32] S. Picozzi, A. Continenza, and A. J. Freeman, Phys. Rev. B **69**, 094423 (2004).

[33] G. M. Müller, J. Walowski, M. Djordjevic, G.-X. Miao, A. Gupta, A. V. Ramos, K. Gehrke, V. Moshnyaga, K. Samwer, J. Schmalhorst *et al.*, Nat. Mater. **8**, 56 (2009).

[34] A. Mann, J. Walowski, M. Münzenberg, S. Maat, M. J. Carey, J. R. Childress, C. Mewes, D. Ebke, V. Drewello, G. Reiss, and A. Thomas , Phys. Rev. X. **2**, 041008 (2012).

[35] D. Steil, O. Schmitt, R. Fetzer, T. Kubota, H. Naganuma, M. Oogane, Y. Ando, A. Suszka, O. Idigoras, G. Wolf *et al.*, New. J. Phys. **16**, 063068 (2014).

[36] D. Steil, S. Alebrand, T. Roth, M. Krauß, T. Kubota, M. Oogane, Y. Ando, H. C. Schneider, M. Aeschlimann, and M. Cinchetti, Phys. Rev. Lett. **105**, 217202 (2010).

[37] J.-P. Wüstenberg, D. Steil, S. Alebrand, T. Roth, M. Aeschlimann, and M. Cinchetti, Phys. Status Solidi B **248**, 2330 (2011).

[38] See Supplemental Material at http://link.aps.org/supplemental/10.1103/PhysRevB.104.L100408 for computational details regarding exchange interactions, Gilbert damping and atomistic spin dynamics. Experimental details about sample structures, magneto-optical Kerr effect and ferromagnetic resonance.

[39] S. Jana, J. A. Terschlüsen, R. Stefanuik, S. Plogmaker, S. Troisi, R. S. Malik, M. Svanqvist, R. Knut, J. Söderström, and O. Karis, Rev. Sci. Instrum. **88**, 033113 (2017).

[40] S. Mizukami, D. Watanabe, M. Oogane, Y. Ando, Y. Miura, M. Shirai, and T. Miyazaki, J. Appl. Phys. **105**, 07D306 (2009).

[41] A. Kumar, F. Pan, S. Husain, S. Akansel, R. Brucas, L. Bergqvist, S. Chaudhary, and P. Svedlindh, Phys. Rev. B **96**, 224425 (2017).

[42] In Ref. [41] the room temperature FMR data does not show the trend we are reporting here. This has later been found to be related to the limited frequency range studied in that paper. For this paper we have repeated the FMR measurements with a more extended frequency range, and now find the same trends at room temperature as at low temperatures, i.e., Gilbert damping decreases monotonously with increasing growth temperature.

[43] P. Hohenberg and W. Kohn, Phys. Rev. **136**, B864 (1964).

[44] W. Kohn and L. J. Sham, Phys. Rev. **140**, A1133 (1965).

[45] B. Skubic, J. Hellsvik, L. Nordström, and O. Eriksson, J. Phys.: Condens. Mattter. **20**, 315203 (2008).

[46] H. Ebert, D. Ködderitzsch, and J. Minár, Rep. Prog. Phys. **74**, 096501 (2011).

[47] P. Soven, Phys. Rev. **156**, 809 (1967).

[48] G. M. Stocks, W. M. Temmerman, and B. L. Gyorffy, Phys. Rev. Lett. **41**, 339 (1978).

[49] S. H. Vosko, L. Wilk, and M. Nusair, Can. J. Phys. **58**, 1200 (1980).

[50] M. Belmeguenai, H. Tuzcuoglu, M. Gabor, T. Petrisor, C. Tiusan, D. Berling, F. Zighem, and S. M. Chérif, J. Magn. Magn. Mater. **373**, 140 (2015).

[51] H. Ebert, S. Mankovsky, D. Ködderitzsch, and P. J. Kelly, Phys. Rev. Lett. **107**, 066603 (2011).

[52] H. Ebert, S. Mankovsky, K. Chadova, S. Polesya, J. Minár, and D. Ködderitzsch, Phys. Rev. B **91**, 165132 (2015).

[53] W. H. Butler, Phys. Rev. B **31**, 3260 (1985).

[54] A. Liechtenstein, M. Katsnelson, V. Antropov, and V. Gubanov, J. Magn. Magn. Mater. **67**, 65 (1987).

[55] H. Ebert and S. Mankovsky, Phys. Rev. B **79**, 045209 (2009).

[56] P. Tengdin, C. Gentry, A. Blonsky, D. Zusin, M. Gerrity, L. Hellbrück, M. Hofherr, J. Shaw, Y. Kvashnin, E. K. Delczeg-Czirjak *et al.*, Sci. Adv. **6**, eaaz1100 (2020).

[57] I. Turek, J. Kudrnovský, V. Drchal, P. Bruno, and S. Blügel, Phys. Status. Solidi. B **236**, 318 (2003).
[58] R. Chimata, A. Bergman, L. Bergqvist, B. Sanyal, and O. Eriksson, Phys. Rev. Lett. **109**, 157201 (2012).
[59] S. Anisimov, Sov. Phys. JETP **39**, 375 (1974).
[60] O. Eriksson, A. Bergman, L. Bergqvist, and J. Hellsvik, *Atomistic Spin Dynamics*, *Foundations and Applications* (Oxford University Press, Oxford, 2016).
[61] U. Atxitia, O. Chubykalo-Fesenko, J. Walowski, A. Mann, and M. Münzenberg, Phys. Rev. B **81**, 174401 (2010).
[62] S. Husain, S. Akansel, A. Kumar, P. Svedlindh, and S. Chaudhary, Sci. Rep. **6**, 28692 (2016).
[63] Y. Takamura, R. Nakane, and S. Sugahara, J. Appl. Phys. **105**, 07B109 (2009).
[64] D. Strickland and G. Mourou, Opt. Commun. **55**, 447 (1985).
[65] M. Lewenstein, P. Balcou, M. Y. Ivanov, A. L'Huillier, and P. B. Corkum, Phys. Rev. A. **49**, 2117 (1994).
[66] P. B. Corkum, Phys. Rev. Lett. **71**, 1994 (1993).
[67] M. Hecker, P. M. Oppeneer, S. Valencia, H.-C. Mertins, and C. M. Schneider, J. Electron Spectrosc. Relat. Phenom. **144**, 881 (2005).
[68] S. Plogmaker, J. A. Terschlüsen, N. Krebs, M. Svanqvist, J. Forsberg, U. B. Cappel, J.-E. Rubensson, H. Siegbahn, and J. Söderström, Rev. Sci. Instrum. **86**, 123107 (2015).
[69] R. Stefanuik, R. Knut, S. Jana, J. Terschlüsen, A. Sandell, and J. Söderström, J. Electron Spectrosc. Relat. Phenom. **224**, 33 (2018).
[70] G. Grimvall, *Thermophysical Properties of Materials* (North-Holland, Amsterdam, 1999).
[71] S. Husain, A. Kumar, S. Akansel, P. Svedlindh, and S. Chaudhary, J. Magn. Magn. Mater. **442**, 288 (2017).
[72] R. Gupta, N. Behera, V. A. Venugopal, S. Basu, A. K. Puri, P. Ström, M. A. Gubbins, L. Bergqvist, R. Brucas, P. Svedlindh, and A. Kumar, Phys. Rev. B **101**, 024401 (2020).

Correction: The copyright license statement was presented incorrectly and has been fixed.